High precision measurements of atom column positions using model-based exit wave reconstruction

High Precision Measurements of Atom Column Positions using Model-Based Exit Wave Reconstruction

A. De Backer*, S. Van Aert, D. Van Dyck

Electron Microscopy for Materials Science (EMAT),University of Antwerp, Groenenborgerlaan 171, 2020 Antwerp, Belgium

Abstract

In this paper, it has been investigated how to measure atom column positions as accurately and precisely as possible using a focal series of images. In theory, it is expected that the precision would considerably improve using a maximum likelihood estimator based on the full series of focal images. As such, the theoretical lower bound on the variances of the unknown atom column positions can be attained. However, this approach is numerically demanding. Therefore, maximum likelihood estimation has been compared with the results obtained by fitting a model to a reconstructed exit wave rather than to the full series of focal images. Hence, a real space model-based exit wave reconstruction technique based on the channelling theory is introduced. Simulations show that the reconstructed complex exit wave contains the same amount of information concerning the atom column positions as the full series of focal images. Only for thin samples, which act as weak phase objects, this information can be retrieved from the phase of the reconstructed complex exit wave.

Keywords: High-resolution transmission electron microscopy (HRTEM), Exit wave reconstruction, Parameter Estimation Theory

1. Introduction

High-resolution transmission electron microscopy (HRTEM) is established as a method used in order to determine the internal structure of materials at a local scale [1]. Recently, the introduction of aberration-corrected electron microscopes has improved the interpretability of the images down to atomic resolution [2–5]. Nevertheless, the phase information is lost due to the image recording process, which is a limiting factor since the phase contains significant information on the positions of the atom columns. Therefore, the imaging process has to be inverted numerically in order to calculate the wave function at the exit plane of the object. One commonly applied technique is to use a series of images at different focal values [6–14]. In this way both the amplitude and phase information of the exit wave are recovered. In addition, a better signal-to-noise ratio is achieved and residual lens aberrations are eliminated [9, 12, 13, 15, 16]. The reconstructed exit wave is closely related to the object structure. In combination with quantitative methods, atom column positions can be measured with a precision of a few picometers [2–4, 17–19].

In this paper, a real space model-based approach for exit wave reconstruction based on the channelling theory [20–24] is introduced in order to investigate the precision that can ultimately be obtained for the unknown structure parameters. Quantitative structure determination then becomes a statistical parameter estimation problem in which the available parametric model is fitted to the experimental data using a criterion of goodness of fit [18, 19, 25–28].

In our opinion, the ultimate goal of quantitative HRTEM is to determine structure parameters with the highest possible precision and accuracy. Due to the unavoidable presence of noise in the observations, the estimated parameters will fluctuate from experiment to experiment. The amount of variation in these estimated parameters quantifies the precision. Moreover, modelling errors will limit the accuracy resulting in bias, that is a systematic deviation of the estimated parameters from the true parameters. Statistical parameter estimation theory provides an expression for the highest precision, or in other words, the minimum variance, with which the atom column positions can be determined. This is the so-called Cramér-Rao lower bound (CRLB) [25, 26, 29], which is a theoretical lower bound on the variance of any unbiased estimator of the unknown structure parameters. One of the properties of the maximum likelihood estimator is that it achieves the Cramér-Rao lower bound asymptotically, i.e. for an infinite number of observations. However, determining the parameters using the maximum likelihood estimator applied to the originally recorded focal images is numerically demanding. In current studies, however, only the phase information of the reconstructed exit wave is employed to determine the atom column position parameters using, for example, an empirical parametric model consisting of a superposition of Gaussian peaks [5, 15, 18, 19]. In principle, more accurate and precise results might be expected if the reconstructed amplitude is also taken into account using a physics-based parametric model using the channelling theory. By means of image simulations of an ideal Au [100] sample, which are subject to counting noise, different parameter estimation methods have been compared. It has been investigated what precision could be obtained

*Corresponding author
Email address: Annick.DeBacker@ua.ac.be (A. De Backer)

by using the phase information of the reconstructed exit wave only or by using the full complex exit wave for different specimen thicknesses. This precision has been compared with the attainable precision that could in principle be obtained by applying the maximum likelihood estimator to the full series of focal images. Although these simulations represent an idealistic case, they serve as a reference for model-based exit wave reconstruction and statistical parameter estimation theory of atom column positions. These simulations should answer the question whether the use of only the phase information in a quantitative analysis is justified and if the analysis would benefit if the amplitude would be used in addition.
The remainder of this article will be structured as follows. In section 2, the model-based approach for exit wave reconstruction is described. Section 3 briefly explains the concepts of statistical parameter estimation theory. In section 4, a simulation of a Au [100] crystal is considered. Finally, in section 5, conclusions are drawn.

2. Model-Based Exit Wave Reconstruction

In this paper, we consider a real space reconstruction technique in contrast to existing techniques which act in Fourier space [7–9, 11, 12, 30]. The image intensities of the focal series are backpropagated to the zero-focus to reconstruct the wave at the exit face of the specimen. Next, the set of backpropagated images is averaged. The real space approach for exit wave reconstruction is very intuitive and understandable, but is conceptually different from the existing focal series reconstruction methods. In most reconstruction methods the only aim is to reconstruct the complex exit wave as such. However, since it is the purpose to derive also the crystal structure from the exit wave, we want to go one step further and include also the channelling theory for the electron interaction already in the exit wave. For this purpose a real space approach for focal series reconstruction is much more suitable.
The channelling theory [20–23] describes the quantum mechanical interaction of the electrons with the object and provides a closed analytical expression for the exit wave which is parametric in the structure parameters. The complex exit wave of an object consisting of M atom columns described in the channelling theory consists of a vacuum wave and an interaction wave [20–23]:

$$\begin{aligned}\psi_{\text{ex}}(\mathbf{r},z) =& 1+\psi_{\text{int}}(\mathbf{r},z)\\ =& 1+\sum_{m=1}^{M} c_m\phi_{1s,m}(\mathbf{r}-\boldsymbol{\beta}_m)\left[\exp\left(-i\pi\frac{E_{1s,m}}{E_0}\frac{1}{\lambda}z\right)-1\right]\end{aligned} \tag{1}$$

where $\mathbf{r}=(x,y)^T$ is a two-dimensional vector in the exit plane of the object, perpendicular to the incident beam direction; E_0 denotes the incident electron energy, λ the electron wavelength and z the object thickness; $\phi_{1s,m}(\mathbf{r}-\boldsymbol{\beta}_m)$ is the eigenfunction of the lowest energy bound state with energy $E_{1s,m}$, i.e. the 1s-state of an atom column m at position $\boldsymbol{\beta}_m=(\beta_{x_m},\beta_{y_m})^T$:

$$\phi_{1s,m}(\mathbf{r}-\boldsymbol{\beta}_m)=\frac{1}{a_m\sqrt{2\pi}}\exp\left(-\frac{r^2}{4a_m^2}\right) \tag{2}$$

where a_m is the column dependent width. Moreover, r is the Euclidean norm of the vector $\mathbf{r}-\boldsymbol{\beta}_m$, which is defined as:

$$r=\|\mathbf{r}-\boldsymbol{\beta}_m\|_2=\sqrt{(x-\beta_{x_m})^2+(y-\beta_{y_m})^2} \tag{3}$$

The interpretation of expression (1) for the exit wave is as follows. Each atom column acts as a channel in which the wave function oscillates periodically with depth [20, 24]. This periodicity is related to the average mass density of an atom column and is given by:

$$D_{1s}=\left|\frac{2E_0\lambda}{E_{1s,m}}\right| \tag{4}$$

This distance is called the extinction distance. The importance of this result lies in the fact that it can be used to describe the dynamical diffraction up to larger thicknesses than the usual phase grating approximation [20, 24].
The wave function in the image plane is given by the exit wave convoluted with a point spread function accounting for the effect of defocus ϵ and spherical aberration C_s [31]:

$$\psi_{\text{im}}(\mathbf{r},z;C_s,\epsilon)=1+\psi_{\text{int}}(\mathbf{r},z)*p_{C_s}(\mathbf{r};C_s)*p_{\epsilon}(\mathbf{r};\epsilon) \tag{5}$$

The intensity in the image plane is described by [31]:

$$I(\mathbf{r},z;C_s,\epsilon)=|\psi_{\text{im}}(\mathbf{r},z;C_s,\epsilon)|^2 \tag{6}$$

The intensity is the modulus squared of the image wave; other aberration effects are neglected in the simulations as it is assumed that they can be numerically corrected in the reconstruction [7, 11–13, 32]. The expression (6) for the image intensity can be written as a sum of 4 terms: a constant, linear, conjugate linear and non-linear term.
In order to reconstruct the exit wave, the image intensities of the focal series are backpropagated. This backpropagation is performed by a convolution with the inverse point spread function of the defocus $p_{\epsilon}^{-1}(\mathbf{r};\epsilon)=p_{\epsilon}^{*}(\mathbf{r};\epsilon)$, which equals the point spread function of the defocus with the opposite focal value $p_{\epsilon}(\mathbf{r};-\epsilon)$. In this way, a compensation is obtained for the effect of the defocus. The same procedure can be applied for spherical aberration resulting into the following expression:

$$\begin{aligned}\Psi_{\text{rec}}(\mathbf{r},z) =& <I(\mathbf{r},z)>\\ =& \frac{1}{N}\sum_{n=-\frac{N-1}{2}}^{\frac{N-1}{2}} I(\mathbf{r},z;C_s,\epsilon_n)*p_{\epsilon}(\mathbf{r},-\epsilon_n)*p_{C_s}(\mathbf{r},-C_s)\end{aligned} \tag{7}$$

The focal value ϵ_n corresponds to the focal value of an image of the focal series. Other aberrations, like incoherence effects present in experimental images can be corrected by including them in the backpropagation by the appropriate inverse point

spread function [11, 33].

Equation (7) demonstrates the procedure for obtaining the reconstructed exit wave $\Psi_{\text{rec}}(\mathbf{r}, z)$. The reconstructed exit wave $\Psi_{\text{rec}}(\mathbf{r}, z)$ can be calculated by working out the right-hand side of equation (7) after substitution of equation (5) and (6). This calculation results into 4 contributions: a constant, a linear, a conjugate linear and a non-linear term. Under some approximations (see Appendix Appendix A), an explicit analytical expression can be obtained. In the ideal case, this reconstructed exit wave Ψ_{rec} equals the theoretical exit wave $\psi_{\text{ex}}(\mathbf{r}, z)$. The sum of the reconstructed constant and linear term indeed yields the expression for the exit wave provided by the channelling theory, i.e. expression (1). It can be shown that the conjugate linear term yields a constant background in the limit of an infinite series of focal images. Although it is likely that the non-linear term is small compared to the constant and linear contribution, it is more difficult to interpret. A numerical evaluation of the reconstructed wave is useful to determine the importance of the different terms as a function of some experimental parameters. From such an analysis, it follows that the contribution of the non-linear term becomes more and more negligible when:

- the *mean focal value* of the focal series is selected away from the zero-focus;
- the *number of images* of the focal series is increased using a small defocus step to ensure sufficient sampling;
- the *spherical aberration constant* increases.

This result means that for focal series where the mean focal value is chosen away from the zero-focus or where a non-zero spherical aberration constant is chosen, the reconstructed exit wave better matches the true exit wave. This is shown in figure 1, where the sum over the pixel values of the squared bias map between the reconstructed exit wave ψ_{rec} and the true exit wave ψ_{ex} of the channelling theory is plotted as a function of the spherical aberration constant and the mean defocus of the focal series. The figure is calculated for an isolated Si[100] atom column in reconstructions obtained from a simulated focal series with 21 focal images and a focal step of 2.5 nm. The thickness of the simulated object equals half the extinction distance, $0.5D_{1s}$; the object parameters for Si[100] are given in table 1. For other thicknesses similar figures can be obtained for comparing the amplitude and phase of the reconstructed exit wave with the true exit wave. Moreover, simulation results show that the quality of the reconstructed exit wave also depends on the atom column type: the reconstruction is better for heavier atom columns.

In figure 2, a simulation demonstrates that the reconstructed exit wave shows good agreement with the true input exit wave for a realistic set of experimental parameters in a focal series. A focal series of 21 images is simulated for a Au [100]-crystal with a thickness of $0.1D_{1s}$ having a mean focal value of -75 nm, a focal step of 2.5 nm and a spherical aberration constant of 0.5 mm. The object parameters for Au[100] are also given in table 1. The two-dimensional projected structure is modelled as a lattice of 7×7 projected atom columns based on

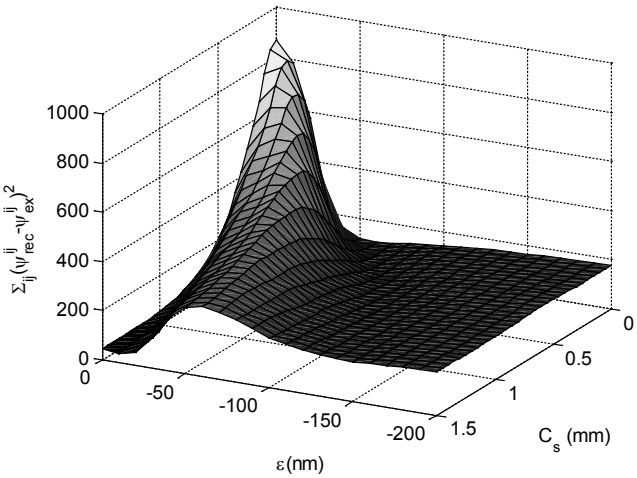

Figure 1: Sum of the squared bias map between the reconstructed exit wave ψ_{rec} and the true exit wave ψ_{ex} of an isolated Si[100] atom column as a function of the spherical aberration constant C_s and the mean defocus ϵ of the focal series. Increasing the focal value leads to a better agreement with the true exit wave.

parameter	Si[100]	Au[100]
Z (atomic number)	14	79
a_m Å	0.34	0.13
$E_{1s,m}$ (eV)	-20.2	-210.8
d Å(interatomic distance)	5.43	4.08
D_{1s} (nm)	59.4	5.7
D_{1s} (atoms)	109	14

Table 1: Object parameters used in the simulation of the focal series.

the channelling model. The phase and amplitude of the reconstructed wave and the true exit wave are compared in figures 2(a) and 2(b), respectively. Also for thicker specimens, the reconstructed exit wave will show good agreement with the true input exit wave. This agreement enables us to use the parametric model from the channelling theory given by equation (1), in a statistical parameter estimation procedure applied to the reconstructed exit wave.

3. Statistical Parameter Estimation Theory

3.1. Principle

The reconstructed exit wave does not directly provide quantitative measurements of the atom column positions. Therefore, the reconstructed exit wave is used as a starting point for measurement of the atom column positions using statistical parameter estimation theory. In this way, it is possible to determine the atom column positions with a precision that is orders of magnitude better than the information limit of the electron microscope. This requires a quantitative model-based method, in which the focal series or the reconstructed exit wave is considered as a data plane from which the unknown structure parameters, such as the atom column positions, have to be estimated in a statistical way [29]. For a successful application, a parametric model describing the expectations of the pixel values in

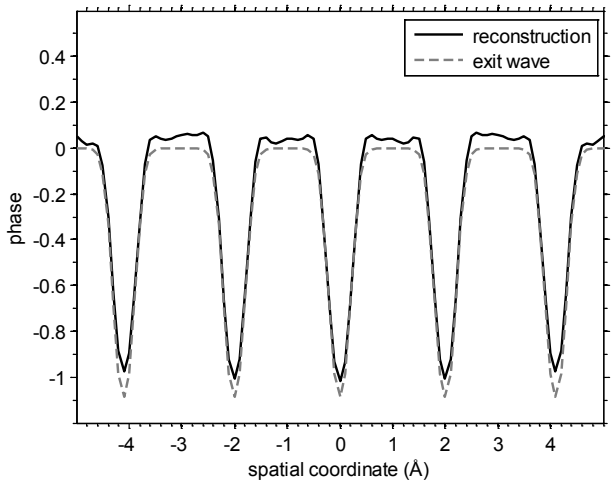

(a) phase

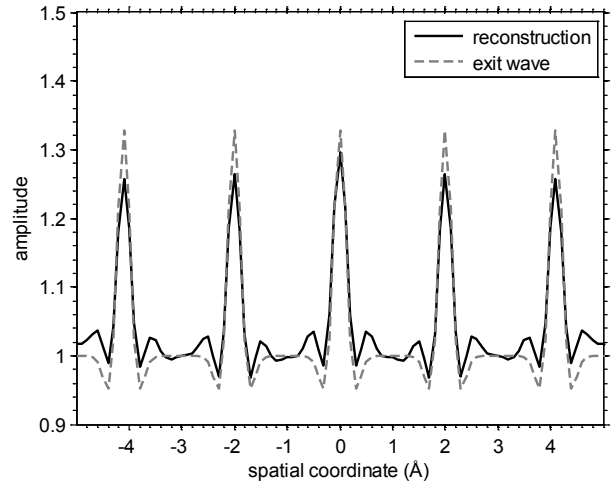

(b) amplitude

Figure 2: Comparison of the phase (left) and amplitude (right) of the reconstructed exit wave with the input wave modelled with the channelling theory represented as line plots through the atom column positions of a Au[100] crystal.

the focal series or in the real and imaginary part of the complex exit wave should be available. Our goal for quantitative interpretation of HRTEM images is to obtain numbers with the highest possible precision and accuracy. Statistical parameter estimation theory provides an expression for the highest possible precision in the form of a lower bound on the variance with which the structure parameters can be estimated unbiasedly [29]. This lower bound is independent of the parameter estimation method that is used. In practice, different estimators can be used to estimate the same parameters. However, the variance of unbiased estimators will never be lower than the Cramér-Rao lower bound. By comparing this lower bound with the sample variance of the estimated parameters such as the atom column positions, it can be examined if all information contained in the images of the focal series is extracted using a particular estimation procedure. In Appendix B, the concept of Fisher information and the Cramér-Rao lower bound is summarised [25, 26, 29].

3.2. Estimation of atom column positions

The maximum likelihood estimator, which is briefly discussed in Appendix B, achieves the Cramér-Rao lower bound asymptotically, i.e. for an increasing number of observations. The Cramér-Rao lower bound can thus be attained by deriving the maximum likelihood estimates from the full series of focal images. In other words, the maximum likelihood estimator seems to be the most preferable estimator in terms of precision. However, deriving the maximum likelihood estimates from a full series of focal images is not practically useful because of the numerical complexity of the problem. Therefore, least squares estimates are often derived from the phase of the reconstructed exit wave assuming an empirical parametric model. Nevertheless, it is expected that the precision would improve when deriving the least squares estimates from the full complex exit wave rather than from the phase of the exit wave only. In the following subsections, the least squares estimation procedures when using the phase of the exit wave only or when using the full complex exit wave will be outlined. In section 4, the performance of these estimators will be studied. In particular, we will compare the precision of these estimators with the attainable precision, given by the Cramér-Rao lower bound.

3.2.1. Least squares estimator using phase of reconstructed exit wave

It is generally known that the phase of the exit wave is peaked at the atom column positions. Accordingly, an empirical model is often used in current studies in which the phase is modelled as a superposition of Gaussian functions which are peaked at the atom column positions [5, 15, 18, 19]. Therefore, the expectation at the pixel (k, l) at the position (x_k, y_l) of the phase of the exit wave can be described as:

$$f_{kl}^{\mathrm{p}}(\boldsymbol{\vartheta}) = \zeta + \sum_{i=1}^{I} \sum_{m_i=1}^{M_i} \eta_{m_i} \exp\left(-\frac{(x_k - \beta_{x_{m_i}})^2 + (y_l - \beta_{y_{m_i}})^2}{2\rho_i^2} \right) \quad (8)$$

where the superscript p refers to the model for the phase; ζ is a constant background, ρ_i is the width of the Gaussian peak, η_{m_i} is the height of the Gaussian peak and $\beta_{x_{m_i}}$ and $\beta_{y_{m_i}}$ are the x- and y-coordinate of the m_ith atom column, respectively. The index i refers to a particular atom type, with I the total number of different atom types and m_i refers to the mth atom column of atom type i with M_i the total number of atom columns for atom type i. The unknown parameters of the model:

$$\boldsymbol{\vartheta} = (\beta_{x_{1_1}}, \ldots, \beta_{x_{M_I}}, \beta_{y_{1_1}}, \ldots, \beta_{y_{M_I}}, \rho_1, \ldots, \rho_I, \eta_{1_1}, \ldots, \eta_{M_I}, \zeta)^T \quad (9)$$

are estimated in the least squares sense. The uniformly weighted least squares estimates $\hat{\boldsymbol{\vartheta}}$ are given by the values of t that minimise the uniformly weighted least squares criterion:

$$\hat{\boldsymbol{\vartheta}} = \arg\min_{t} \sum_{k=1}^{K} \sum_{l=1}^{L} (w_{kl} - f_{kl}^{\mathrm{p}}(t))^2 \quad (10)$$

with w_{kl} the value of the reconstructed phase at the pixel (k, l).

3.2.2. Least squares estimator using phase and amplitude of reconstructed exit wave

In order to attain a higher precision, especially for thicker specimens, all the information available in the reconstructed exit wave, i.e. phase and amplitude information, can be used to estimate the unknown parameters. The implementation for the complex exit wave is fully equivalent to the procedure for the phase, although more extended. The complex exit wave is given by expression (1). This physics-based parametric model for this complex exit wave can be rewritten and separated in a real ($\mathcal{R}$) and imaginary ($\mathcal{I}$) part:

$$\begin{aligned} f^{\mathrm{c}}_{kl}(\boldsymbol{\vartheta}) =& \mathcal{R}(\boldsymbol{\vartheta}) + i\mathcal{I}(\boldsymbol{\vartheta}) \\ =& \left[\zeta_{\mathcal{R}} + \sum_{i=1}^{I}\sum_{m_i=1}^{M_i} \eta^{\mathcal{R}}_{m_i} \exp\left(-\frac{(x_k - \beta_{x_{m_i}})^2 + (y_l - \beta_{y_{m_i}})^2}{2\rho_i^2}\right)\right] \\ &+ i\left[\zeta_{\mathcal{I}} + \sum_{i=1}^{I}\sum_{m_i=1}^{M_i} \eta^{\mathcal{I}}_{m_i} \exp\left(-\frac{(x_k - \beta_{x_{m_i}})^2 + (y_l - \beta_{y_{m_i}})^2}{2\rho_i^2}\right)\right] \end{aligned} \tag{11}$$

where the superscript c refers to the model for the complex wave. The effect of the thickness of the object is incorporated in the parameters $\eta^{\mathcal{R}}_{m_i}$ and $\eta^{\mathcal{I}}_{m_i}$. The vector containing the unknown parameters for the complex model is:

$$\begin{aligned} \boldsymbol{\vartheta} =& (\beta_{x_{1_1}}, \ldots, \beta_{x_{M_I}}, \beta_{y_{1_1}}, \ldots, \beta_{y_{M_I}}, \rho_1, \ldots, \rho_I, \\ & \eta^{\mathcal{R}}_{1_1}, \ldots, \eta^{\mathcal{R}}_{M_I}, \eta^{\mathcal{I}}_{1_1}, \ldots, \eta^{\mathcal{I}}_{M_I}, \zeta_{\mathcal{R}}, \zeta_{\mathcal{I}})^T \end{aligned} \tag{12}$$

Minimisation of the uniformly weighted least squares criterion yields the estimated parameters:

$$\hat{\boldsymbol{\vartheta}} = \arg\min_{t} \sum_{k=1}^{K}\sum_{l=1}^{L} \left[(w^{\mathcal{R}}_{kl} - \mathcal{R}(\mathbf{t}))^2 + (w^{\mathcal{I}}_{kl} - \mathcal{I}(\mathbf{t}))^2\right] \tag{13}$$

where $w^{\mathcal{R}}_{kl}$ and $w^{\mathcal{I}}_{kl}$ represent the real and imaginary part of the reconstructed complex exit wave respectively.

4. Simulations of Au [100]

4.1. Attainable precision

Given the asymptotic properties of the maximum likelihood estimator, it is expected that the lower bound on the variance of the unknown parameters can be attained by applying the maximum likelihood estimator to the originally recorded focal images. However, this approach is unpractical and computationally demanding. In this section, the variance of the structure parameters obtained when applying the uniformly weighted least squares estimator is examined and compared with the lower bound on the variance. In order to derive the Cramér-Rao lower bound on the variance of the unknown parameters, the model describing the expectations of the original observations of the focal series is needed. The expectation model for the image intensity of an image of the recorded focal series used for this purpose equals:

$$f^{\mathrm{i}}_{kl}(\boldsymbol{\vartheta}) = \lambda^{n}_{kl} = N_d \frac{I(\mathbf{r}, z; C_s, \epsilon_n)}{I_{\mathrm{norm}}} \Delta x \Delta y \tag{14}$$

where the superscript i refers to the model for the image intensity. This result defines the number of electrons expected to be found at a pixel (k, l) taking into account the electron dose. In this equation, $I(\mathbf{r}, z; C_s, \epsilon_n)$ denotes the intensity in the image plane as given by expression (6), N_d the total number of detected electrons and Δx and Δy represent the sampling distances in the x- and y-direction. The normalisation factor I_{norm} is given by:

$$I_{\mathrm{norm}} = \int I(\mathbf{r}, z; C_s, \epsilon_n) d\mathbf{r} \tag{15}$$

where the integral extends over the whole field of view. Under the assumption that the image intensities are Poisson distributed, the Cramér-Rao lower bound on the variance is given by the inverse Fisher information matrix of which the elements are given by expression (B.3). The derivatives in expression (B.3) are calculated with respect to the parameters $\boldsymbol{\vartheta}$ in the expectation model given by equation (14), i.e. the positions, the width and the height of the atom columns and a constant background. Following equation (B.5), the diagonal elements of the inverse Fisher information matrix define lower bounds on the variance of the parameters $\boldsymbol{\vartheta}$. The thus obtained numbers will be compared with the variance of the structure parameters estimated from the phase of the reconstructed exit wave and estimated from the reconstructed complex exit wave. This comparison is first carried out for an isolated atom column and next for an assembly of atom columns. Furthermore, the comparison is done for different specimen thicknesses. For thin specimens for which the weak phase object approximation (WPOA) is valid, most object information will be contained in the phase of the reconstructed exit wave. The weak phase object approximation is valid if [20, 23]:

$$|E_{1s,m}| < \frac{E_0 \lambda}{\pi z}. \tag{16}$$

In terms of the extinction distance D_{1s} (expression (4)), the weak phase object approximation is valid if the specimen thickness is smaller than $0.16 D_{1s}$. For Au[100], the extinction distance D_{1s} equals 5.7 nm, i.e. about 14 atoms. This means that the WPOA is valid for a specimen thickness less than 2 atoms. However, it should be noted that some deviations can be expected from equation (16) for very heavy atoms.

Focal series for different object thicknesses are simulated of an isolated Au[100] atom column and of a 7×7 lattice of projected Au[100] atom columns, modelled using the channelling theory. The microscope parameters for the simulation of the focal series are shown in table 2; the value of C_s is arbitrarily chosen non-zero. Different noise realisations are simulated to investigate the attainability of the lower bound on the variance. The complex exit wave is reconstructed from 100 different Poisson distributed noise realisations of a focal series calculated from

parameter		value
accelerating voltage	V_0 (kV)	300
mean focal value	ϵ (nm)	-75
focal step	γ (nm)	2.5
spherical aberration constant	C_s (mm)	0.5
number of focal images	N	21
pixel size	$\Delta x = \Delta y$ (Å)	0.1
number of pixels x- and y-direction	$K = L$	1024
electron dose	N_d $(e^-\text{Å}^{-2})$	7854

Table 2: Microscope parameters for the simulation of the focal series.

the expectation model given by equation (14). The unknown parameters of the parametric models for the phase of the reconstructed exit wave and the reconstructed complex exit wave, described by expressions (8) and (11) respectively, are estimated in the least squares sense. The sample mean and sample variance are computed from the 100 estimates and compared with the true values and the Cramér-Rao lower bound on the variance of the position parameters, respectively.

4.2. Isolated atom column

In this analysis unbiased estimates have been obtained for the x- and y-coordinates. The results of the analysis of the attainability of the Cramér-Rao lower bound for an isolated atom column as a function of the object thickness are presented in figure 3. The figure shows the ratio of the estimated variance to the calculated Cramér-Rao lower bound for the x- and y-position coordinates. The Cramér-Rao lower bound on the variance of the position parameters also depends on the object thickness as is shown in the inset in figure 3. The attainable precision for the position parameters is highest when the thickness equals half the extinction distance. Here, the electrons are most strongly localised at the atom column positions implying that the exit wave is peaked maximally at the atom positions. From figure 3, it can be concluded that the lower bound on the variance is attained for all thicknesses when the column position coordinates are estimated from the complex reconstructed exit wave using the parametric model given by the channelling theory (equation (11)). This result is also valid for thicknesses larger than $0.5D_{1s}$ and will show a periodic behaviour since the exit wave varies periodically with depth. By estimating the position coordinates from the phase of the reconstructed exit wave using the model of Gaussian peaks (equation (8)), the Cramér-Rao lower bound is only attained when the weak phase approximation is valid, i.e. if the thickness is smaller than $0.16D_{1s}$. It is clear that for larger object thicknesses, for which the WPOA is no longer valid, estimating the position coordinates from the complex reconstructed exit wave is necessary in order to attain the highest possible precision.

4.3. Assembly of atom columns

To evaluate the effect of neighbouring atom columns, a 7×7 lattice of projected Au[100] atom columns is modelled. For an assembly of atom columns two different thicknesses are considered: $z_1 = 0.1D_{1s}$ corresponding to a specimen

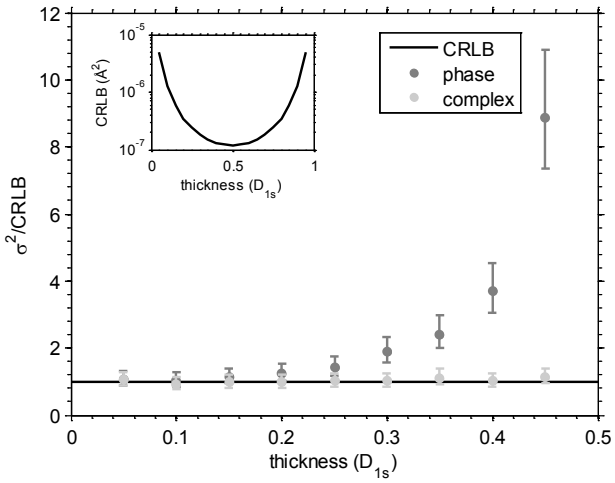

Figure 3: Attainability of the CRLB as a function of the object thickness for an isolated Au[100] atom column. The error bars show the 95% confidence intervals for the estimated variances. The inset shows the CRLB as a function of the object thickness.

thickness of only 1 atom and $z_2 = 0.4D_{1s}$ corresponding to a specimen thickness of 5 atoms. The weak phase approximation is valid for z_1 but not for z_2. The positions of the central 5×5 atom columns are considered in the analysis in order to avoid boundary effects at the outermost atom columns of the simulation. Like for isolated columns, the estimates for the position coordinates are unbiased. The results for the attainability of the CRLB for both thicknesses z_1 and z_2 are presented in figure 4. The ratio of the estimated variance for the x- and y-coordinates to the CRLB are plotted for the 25 atom columns. As expected for the thin object the variances on the position parameters correspond to the theoretical lower bound on the variance for both estimating the position coordinates from the phase information only or from the full complex exit wave. For the thicker object, where the WPOA is no longer valid, the CRLB can only be attained by estimating the position coordinates from the complex model for the exit wave to the reconstructed exit wave. If the position parameters are determined based on the full complex exit wave, the precision is approximately 3 to 4 times better in terms of variance than determining the atom column position parameters from the phase of the reconstruction. This result is in agreement with the result for the isolated atom column.

Note that in practice, the lower bound and estimated variances will be typically larger, since their actual values critically depend on the image contrast. A reduction of contrast will indeed result in a loss of precision [19]. So far, the contrast mechanism in HRTEM images is not yet fully understood. The contrast in experimental images is typically a factor of 3 lower than in simulated images. This is the well-known contrast problem, often referred to as the Stobbs factor [34–36]. Phonon scattering and different experimental conditions, like the stability of the specimen and the microscope, atom thermal vibrations, lattice configuration, residual microscope aberrations, time dependent incoherence may contribute to a

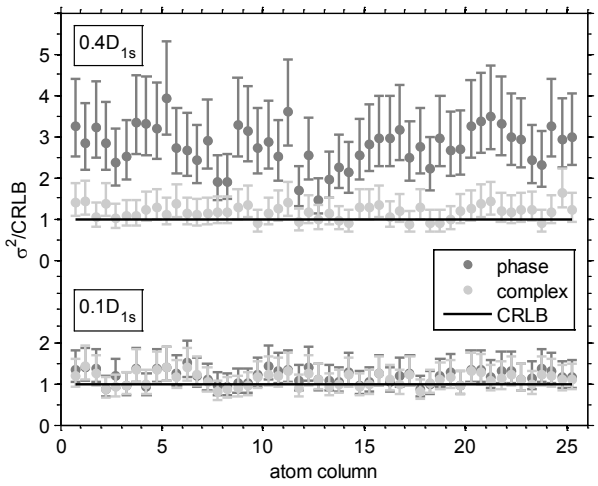

Figure 4: Attainability of the CRLB for 25 position estimates of Au[100] atom columns. The bottom of the graph shows the result for thickness $z_1 = 0.1D_{1s}$ and the top of the graph shows the result for thickness $z_2 = 0.4D_{1s}$. Each atom column position corresponds to two estimated ratios in the graph, the x-coordinate and y-coordinate, resulting in 50 data points on the horizontal axis. The error bars show the 95% confidence intervals for the estimated variances.

loss of image contrast. So far, it is impossible to take all these factors properly into account in the theory.

5. Conclusions

Often only the reconstructed phase is used in quantitative studies of exit waves reconstructed from focal series. However, it is expected that the precision with which unknown structure parameters can be estimated would improve when using the amplitude of the exit wave as well. Therefore, the performance of both approaches has theoretically been examined in this study in terms of the attainable precision and bias by means of simulations. This has been done using a model-based approach for exit wave reconstruction using the channelling theory. Combined with statistical parameter estimation theory, quantitative measurements were obtained for atom column position parameters and their precision. In a simulation of Au[100], the variance thus attained was compared with the Cramér-Rao lower bound, a theoretical lower bound on the variance of unbiased estimators. Although, it was expected that the Cramér-Rao lower bound could only be attained when deriving the maximum likelihood estimates from the full series of focal images, it has been demonstrated that the reconstructed complex exit wave contains the same amount of information on the position parameters. Estimating the position parameters from the complex exit wave using the parametric model from the channelling theory results in the highest possible precision. This precision cannot be obtained when using the phase information only except for thin specimens where the weak phase approximation is valid, that is, thinner than $0.16D_{1s}$ with D_{1s} the extinction distance. For thicker specimens, an improvement of a factor of about 4 in terms of the variance with which the atom column positions can be estimated is observed, when using the full complex exit wave in the estimation procedure. From this study we can conclude that it is therefore recommendable to use the full complex exit wave to determine quantitative information about the atom column positions.

Acknowledgements

The authors gratefully acknowledge financial support from the Fund for Scientific Research-Flanders (FWO), contract no. G.0188.08.

Appendix A. Analytical expression for the reconstructed exit wave

An analytical expression is calculated for the complex reconstructed exit wave by working out the right-hand side of equation (7) after substitution of equation (5) and (6), resulting into 4 terms. The expression for the point spread functions are given by:

$$p_\epsilon(\mathbf{r};\epsilon) = \mathcal{F}^{-1}\left\{\exp\left(-i\pi\epsilon\lambda g^2\right)\right\}$$
$$p_{C_s}(\mathbf{r};C_s) = \mathcal{F}^{-1}\left\{\exp\left(-\frac{i\pi C_s\lambda^3 g^4}{2}\right)\right\}$$

where $\mathcal{F}^{-1}$ denotes the inverse Fourier transform and g the norm of the two-dimensional spatial frequency vector. A complete analytical expression for the reconstruction can only be obtained by making some approximations for the non-linear term. Moreover, the influence of the spherical aberration is neglected. The complete result of the complex exit wave in the approximated case is:

$$\begin{aligned}
&\text{reconstruction} = \\
&1 \\
&+\psi_{\text{int}}(\mathbf{r}-\boldsymbol{\beta}_m, z) \\
&+\frac{1}{N}\psi^*_{\text{int}}(\mathbf{r}-\boldsymbol{\beta}_m, z) * \mathcal{F}^{-1}\left\{\exp\left(2\pi i\epsilon\lambda g^2\right)\frac{\sin\left(\pi N\gamma\lambda g^2\right)}{\sin\left(\pi\gamma\lambda g^2\right)}\right\} \\
&+\frac{1}{N\cdot\gamma}|\psi_{\text{int}}(\mathbf{r}-\boldsymbol{\beta}_m, z)|^2 * \\
&\quad\mathcal{F}^{-1}\left\{\exp\left(i\pi\epsilon\lambda g^2\right)\exp\left(-g^2\frac{\epsilon^2\lambda^2}{8a_1^2}\right)\exp\left(\frac{\left(i\pi\lambda g^2 - \frac{g^2\epsilon\lambda^2}{4a_1^2}\right)^2}{4\cdot\left(\frac{g^2\lambda^2}{8a_1^2}+\frac{1}{2\zeta^2}\right)}\right)\right\}
\end{aligned}$$

The first two terms yield the expression of the exit wave of the channelling theory.
This analytical expression is useful to calculate the importance of the different terms as a function of the defocus parameter ϵ and the number of focal images N in the series straightforwardly. In order to determine the importance of the different terms as a function of the spherical aberration constant C_s, which is neglected in the analytical calculation, the contributions of the 4 terms should be calculated based on the reconstruction from a set of simulated image intensities.

Appendix B. Fisher information and attainable precision

The usual way to describe the fluctuating behaviour of images in the presence of noise is by modelling the observations $\mathbf{w}$ as stochastic variables $\boldsymbol{\omega}$ [29]. In our case, the observations are given by the pixel values resulting from the electron counts in the images of the focal series. By definition, each set of observations modelled as stochastic variables is characterised by a joint probability density function $p_{\mathbf{w}}(\omega)$. The joint probability density function defines the expectations, i.e. the mean value of each observation and the fluctuations of the observations about these expectations. The expectation values $\mathbb{E}[\boldsymbol{w}]$ are described by a functional model $f^{\mathrm{i}}_{kl}(\boldsymbol{\vartheta})$, i.e. equation (14), parametric in the quantities to be estimated. For HRTEM images in a focal series, the observations w^n_{kl} are assumed to be statistically independent having a Poisson distribution with the following joint probability density function [26, 27]:

$$p(\omega) = \prod_{n=1}^{N}\prod_{k=1}^{K}\prod_{l=1}^{L}\frac{(\lambda^n_{kl})^{\omega^n_{kl}}}{\omega^n_{kl}!}\exp(-\lambda^n_{kl}) \tag{B.1}$$

where λ^n_{kl} is the expectation value of a pixel, i.e. $\mathbb{E}[\boldsymbol{w}] = \lambda^n_{kl} = f^{\mathrm{i}}_{kl}(\boldsymbol{\vartheta})$; the superscript n denotes the nth image of the focal series. The dependence of the joint probability density function on the unknown parameters defines the Fisher information matrix and the Cramér-Rao lower bound [29, 37]. The concept of the Fisher information is a measure to express quantitatively the amount of information on the unknown structure parameters included in the observations. This Fisher information matrix is defined as:

$$F_{\boldsymbol{\vartheta}} = -\mathbb{E}\left[\frac{\partial^2 \ln p(\mathbf{w};\boldsymbol{\vartheta})}{\partial\boldsymbol{\vartheta}^2}\right] \tag{B.2}$$

The Fisher information matrix for a set of Poisson distributed observations then becomes:

$$F_{rs} = \sum_{n=1}^{N}\sum_{k=1}^{K}\sum_{l=1}^{L}\frac{1}{\lambda^n_{kl}}\frac{\partial\lambda^n_{kl}}{\partial\vartheta_r}\frac{\partial\lambda^n_{kl}}{\partial\vartheta_s} \tag{B.3}$$

Using this concept, it is possible to determine the attainable precision, i.e. the lowest variance with which a parameter can be estimated unbiasedly [29]. An expression can be derived for the lower bound on the variance with which the atom positions can be estimated from a quantitative focal series HRTEM experiment. This lower bound is called the Cramér-Rao lower bound and is independent of the estimation method, but depends on the statistical properties of the observations, the measurement points and mostly of the hypothetical true values of the parameters. The Cramér-Rao inequality, with $\hat{\mathbf{t}}$ an unbiased estimator of $\boldsymbol{\vartheta}$, states [25]:

$$\mathrm{cov}\left(\hat{\mathbf{t}},\hat{\mathbf{t}}\right) \geq F^{-1}_{\boldsymbol{\vartheta}} \tag{B.4}$$

The matrix $F^{-1}_{\boldsymbol{\vartheta}}$ is the Cramér-Rao lower bound on the variance of $\hat{\mathbf{t}}$.
This inequality expresses that the difference between the covariance matrix of any unbiased estimator and the Cramér-Rao lower bound is positive semi-definite. A property of a positive semi-definite matrix is that its diagonal elements cannot be negative. This means that the diagonal elements of $\mathrm{cov}\left(\hat{\mathbf{t}},\hat{\mathbf{t}}\right)$ will always be larger than or equal to to the corresponding diagonal elements of the inverse of the Fisher information matrix. Therefore, the diagonal elements of $F^{-1}_{\boldsymbol{\vartheta}}$ define lower bounds on the variances of the elements of $\hat{\mathbf{t}}$:

$$\mathrm{var}\left(\hat{t}_R\right) \geq \left[F^{-1}_{\boldsymbol{\vartheta}}\right]_{RR} \tag{B.5}$$

where $\hat{t}_R$ is the Rth element of $\hat{\mathbf{t}}$ and $\left[F^{-1}_{\boldsymbol{\vartheta}}\right]_{RR}$ is the (R,R)th element of the inverse of the Fisher information matrix.
In addition, from the probability density function of the observations the maximum likelihood estimator may be derived. The maximum likelihood estimator achieves the Cramér-Rao lower bound asymptotically, i.e. for an infinite number of observations. The maximum likelihood estimates, $\hat{\mathbf{t}}_{ML}$ of the parameters $\boldsymbol{\vartheta}$ are given by the values of $\mathbf{t}$ that maximise the likelihood function $L(\mathbf{t}) := p(\mathbf{w};\mathbf{t})$ with $\mathbf{t}$ independent variables replacing the true parameters and the observations replacing the stochastic variables in the joint probability density function:

$$\hat{\mathbf{t}}_{ML} = \arg\max_t L(\mathbf{t}) = \arg\max_t \ln L(\mathbf{t}) \tag{B.6}$$

[1] J. C. H. Spence, The future of atomic resolution electron microscopy for materials science, Materials Science and Engineering R 26 (1999) 1–49.
[2] K. W. Urban, Studying Atomic Structures by Aberration-Corrected Transmission Electron Microscopy, Science 321 (2008) 506.
[3] C. L. Jia, S. B. Mi, K. Urban, I. Vrejoiu, M. Alexe, D. Hesse, Atomic-scale study of electric dipoles near charged and uncharged domain walls in ferroelectric films, Nature materials 7 (2008) 57–61.
[4] C. L. Jia, S. B. Mi, M. Faley, U. Poppe, J. Schubert, K. Urban, Oxygen octahedron reconstruction in the $SrTiO_3$/$LaAlO_3$ heterointerfaces investigated using aberration-corrected ultrahigh-resolution transmission electron microscopy, Physical Review B 79 (2009) 081405(R).
[5] C. L. Jia, S. B. Mi, K. Urban, I. Vrejoiu, M. Alexe, D. Hesse, Effect of a Single Dislocation in a Heterostructure Layer on the Local Polarization of a Ferroelectric Layer, Physical Review Letters 102 (2009) 117601.
[6] D. Van Dyck, M. Op de Beeck, New direct methods for phase and structure retrieval in HREM, in: Proc. XIIth Int. Congress on Electron Microscopy, San Fransisco Press, Seattle, 1990, pp. 26–27.
[7] W. M. J. Coene, A. Thust, M. Op de Beeck, D. Van Dyck, Maximum-likelihood method for focus-variation image reconstruction in high resolution transmission electron microscopy, Ultramicroscopy 64 (1996) 109–135.
[8] M. Op de Beeck, D. Van Dyck, W. Coene, Wave function reconstruction in HRTEM: the parabola method, Ultramicroscopy 64 (1996) 167–183.
[9] A. Thust, W. M. J. Coene, M. Op de Beeck, D. Van Dyck, Focal-series reconstruction in HRTEM: simulation studies on non-periodic objects, Ultramicroscopy 64 (1996) 211–230.
[10] L. J. Allen, M. P. Oxley, Phase retrieval from series of images obtained by defocus variation, Optics Communications 199 (2001) 65–75.
[11] L. J. Allen, W. McBride, N. L. O'Leary, M. P. Oxley, Exit wave reconstruction at atomic resolution, Ultramicroscopy 100 (2004) 91–104.
[12] R. R. Meyer, A. I. Kirkland, W. O. Saxton, A new method for the determination of the wave aberration function for high resolution TEM 1. Measurement of the symmetric aberrations, Ultramicroscopy 92 (2002) 89–109.
[13] A. I. Kirkland, R. R. Meyer, "Indirect" High-Resolution Transmission Electron Microscopy: Aberration Measurement and Wavefunction Reconstruction, Microscopy and Microanalysis 10 (2004) 401–413.
[14] W.-K. Hsieh, F.-R. Chen, J.-J. Kai, A. I. Kirkland, Resolution extension and exit wave reconstruction in complex HREM, Ultramicroscopy 98 (2004) 99–114.
[15] L. Houben, A. Thust, K. Urban, Atomic-precision determination of the reconstruction of a 90° tilt boundary in $YBa_2Cu_3O_{7-\delta}$ by aberration corrected HRTEM, Ultramicroscopy 106 (2006) 200–214.

[16] R. Erni, M. D. Rossell, P. N. H. Nakashima, Optimization of exit-plane waves restored from HRTEM through-focal series, Ultramicroscopy 110 (2010) 151–161.
[17] X. Xu, S. P. Beckman, P. Specht, E. R. Weber, D. C. Chrzan, R. P. Erni, I. Arslan, N. Browning, A. Bleloch, C. Kisielowski, Distortion and Segragation in a Dislocation Core Region at Atomic Resolution, Phys. Rev. Lett. 95 (2005) 145501.
[18] S. Bals, S. Van Aert, G. Van Tendeloo, D. Ávila-Brande, Statistical Estimation of Atomic Positions from Exit Wave Reconstruction with a Precision in the Picometer Range, Phys. Rev. Lett. 96 (2006) 096106.
[19] S. Van Aert, L. Y. Chang, S. Bals, A. I. Kirkland, G. Van Tendeloo, Effect of amorphous layers on the interpretation of restored exit waves, Ultramicroscopy 109 (2009) 237–246.
[20] D. Van Dyck, M. Op de Beeck, A simple intuitive theory for electron diffraction, Ultramicroscopy 64 (1996) 99–107.
[21] D. Van Dyck, J. H. Chen, Towards an exit wave in closed analytical form, Acta Crystallograph. A55 (1999) 212–115.
[22] P. Geuens, D. Van Dyck, The S-state model: a work horse for HRTEM, Ultramicroscopy 93 (2002) 179–198.
[23] P. Geuens, D. Van Dyck, The S-State Model for Electron Channeling in High-Resolution Electron Microscopy, Advances in Imaging and Electron Physics 136 (2005) 111–226.
[24] S. Van Aert, P. Geuens, D. Van Dyck, C. Kisielowski, J. R. Jinschek, Electron channelling based crystallography, Ultramicroscopy 107 (2007) 551–558.
[25] A. van den Bos, Parameter estimation for scientists and engineers, Wiley, 2007.
[26] A. J. den Dekker, S. Van Aert, A. van den Bos, D. Van Dyck, Maximum likelihood estimation of structure parameters from high resolution electron microscopy images. Part I: a theoretical framework, Ultramicroscopy 104 (2005) 83–106.
[27] S. Van Aert, A. J. den Dekker, A. van den Bos, D. Van Dyck, Maximum likelihood estimation of structure parameters from high resolution electron microscopy images. Part II: a practical example, Ultramicroscopy 104 (2005) 107–125.
[28] S. Van Aert, J. Verbeeck, R. Erni, S. Bals, M. Luysberg, D. Van Dyck, G. Van Tendeloo, Quantitative atomic resolution mapping using high-angle annular dark field scanning transmission electron microscopy, Ultramicroscopy 109 (2009) 1236–1244.
[29] A. van den Bos, A. J. den Dekker, Resolution reconsidered - Conventional approaches and an alternative, in: P. Hawkes (Ed.), Advances in Imaging and Electron Physics, Vol. 117, Academic Press, San Diego, USA, 2001, pp. 241–360.
[30] W. Coene, G. Janssen, M. Op de Beeck, D. Van Dyck, Phase Retrieval through Focus Variation for Ultra-Resolution in Field-Emission Transmission Electron Microscopy, Physical Review Letters 69 (1992) 3743.
[31] D. Van Dyck, High-Resolution Electron Microscopy, Advances in Imaging and Electron Physics 123 (2002) 105–171.
[32] L. J. Allen, W. McBride, N. L. O'Leary, M. P. Oxley, Investigation of the effects of partial coherence on exit wave reconstruction, Journal of Microscopy 216 (2004) 70–75.
[33] A. F. de Jong, D. Van Dyck, Ultimate resolution and information in electron microscopy II. The information limit of transmission electron microscopes, Ultramicroscopy 49 (1993) 66–80.
[34] M. J. Hÿtch, W. M. Stobbs, Quantitative comparison of high resolution TEM images with images simulations, Ultramicroscopy 53 (1994) 191–203.
[35] C. B. Boothroyd, Why don't high-resolution simulates and images match?, Journal of Microscopy 190 (1998) 99–108.
[36] A. Thust, High-resolution transmission electron microscopy on an absolute contrast scale, Phys. Rev. Lett. 102 (2009) 220801.
[37] R. I. Jennrich, An Introduction to Computational Statistics-Regression Analysis, Prentice-Hall, Englewood Cliffs, NJ, 1995.